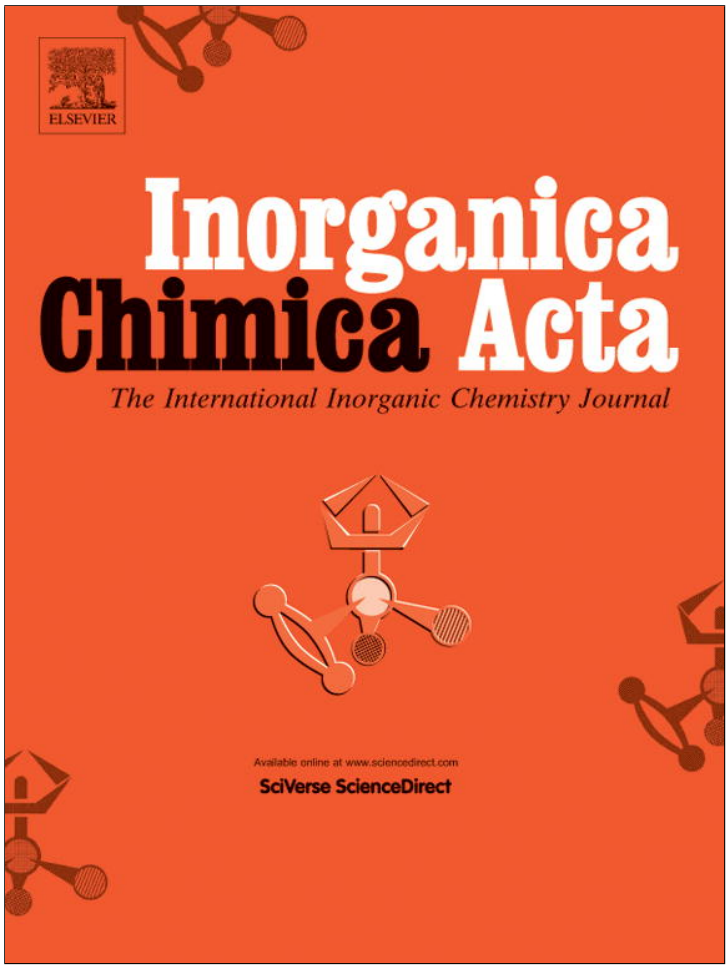

(This is a sample cover image for this issue. The actual cover is not yet available at this time.)

Inorganica Chimica Acta 394 (2013) 229–236

Contents lists available at SciVerse ScienceDirect

Inorganica Chimica Acta

journal homepage: www.elsevier.com/locate/ica

Crystal structure and magnetic properties of two new zoledronate complexes: A Mn dimer [Mn(II)(H_3Zol)$_2$·(H_2O)$_2$] and a Fe_{15} molecular cluster [Fe(III)$_{15}$(HZol)$_{10}$(H_2Zol)$_2$ (H_2O)$_{12}$(Cl_4:(H_2O)$_2$)·Cl_7·(H_2O)$_{65}$] (where H_4Zol: $C_5H_{10}N_2O_7P_2$ is zoledronic acid)

Eleonora Freire [a,b,*,1], Mariano Quintero [a,b,1], Daniel Vega [a,b], Ricardo Baggio [a]

[a] Gerencia de Investigación y Aplicaciones, Centro Atómico Constituyentes, Comisión Nacional de Energía Atómica. Av. Gral Paz 1499, 1650 San Martín, Buenos Aires, Argentina
[b] Escuela de Ciencia y Tecnología, Universidad Nacional General San Martín, Martín de Irigoyen 3100, 1650 San Martín, Buenos Aires, Argentina

ARTICLE INFO

Article history:
Received 3 May 2012
Received in revised form 19 June 2012
Accepted 26 June 2012
Available online 3 August 2012

Keywords:
Zoledronate complexes
Fe_{15} iron cluster
Magnetic behaviour

ABSTRACT

The synthesis, X-ray structure and magnetic properties of two new zoledronato complexes are presented: Mn(II)(H_3Zol)$_2$(H_2O)$_2$, (I) and Fe(III)$_{15}$(HZol)$_{10}$(H_2Zol)$_2$ (H_2O)$_{24}$ (2/3Cl:1/3H_2O)$_6$·7Cl·65(H_2O) (II), where H_4Zol = zoledronic acid = $C_5H_{10}N_2O_7P_2$. Complex (I) is a dimer, built up around an inversion centre where the cation is located, surrounded by two chelating zoledronate anions and two water molecules. The structure is isomorphous to the Co, Ni and Zn isologues. A quite different structure is the Fe(III) complex which consists of a centrosymmetric cluster with 15 Fe(III) cations (one of them at the inversion centre), 12 zoledronate anions, in different protonation states and 26 coordinated water molecules, 24 of which show full occupancy and the remaining 2 share 6 coordination sites with 4 chlorine anions. There are in addition 7 chlorine counterions and a not well determined number of hydration water molecules, their number being adjusted as to match the chemical and TGA analysis. The general shape of the molecule is that of a 6 arm propeller with a Fe(III) cation at its center and two FeO_6 coordination polyhedra sitting above and below, defining some sort of "paddle wheel axis", perpendicular to the wheel plane. Around this axis there is an almost perfect circular structure formed by other six FeO_6 octahedra, to which the "paddles", defined by the remaining six FeO_6 groups attach. The ensemble presents some unusual (Fe···OPO)$_n$ loops (n = 2,3,4), some of them unreported, and displays a striking non-crystallographic −3 symmetry. The protonation state of the zoledronato ligands were inferred from the counterions effectively found and charge balance considerations. Both compounds present a paramagnetic behaviour at R.T, and obey a Curie Weiss law down to rather low temperatures (15 K for (I), 100(K) for (II)) with a tendency to different types of interactions viz., ferromagnetic for (I) and antiferromagnetic for (II). The geometry of the F_{15} cluster is analyzed.

1. Introduction

The area of polynuclear TM clusters (TM, transition metals in general, and focused to Mn(II), Fe(III) in the present discussion), is of relevance in synthetic and structural chemistry due to the possibility of generating molecules with 'programmable' function e.g. as biological mimics [1] and catalysts [2] and physical properties, e.g. non-linear optics [3] and magnetism [4,5]. Novel polynuclear iron clusters with primarily oxygen coordination are active areas of current chemical research [6,7] mainly due to its presence in several metalloenzymes and metalloproteins (see, for instance, [8,9]). Moreover, manganese and iron assemblies have shown interesting properties as molecular magnets [10,11], and an important goal seems to be the development of ligands which might give rise to novel clusters, in order to rationalize their geometry, nuclearity and topologies. In these crystal engineering processes highly branched ligands with multiple chelating arms are the ones to be preferred, since they have the potential to facilitate the formation of cluster-based building blocks and eventually organize them into arrays. This requires many potential chelating groups to both form a polynuclear cluster, and then allow extended interactions between clusters within the array.

A potentially useful family of ligands of this sort is that of bisphosphonates (BPs), a class of osteotropic compounds very effective in treating benign and malignant skeletal diseases (osteoporosis,

* Corresponding author at: Gerencia de Investigación y Aplicaciones, Centro Atómico Constituyentes, Comisión Nacional de Energía Atómica. Av. Gral Paz 1499, 1650 San Martín, Buenos Aires, Argentina. Tel.: +54 11 6772 7097; fax: +54 11 5772 7121.
E-mail address: freire@tandar.cnea.gov.ar (E. Freire).
[1] Member of Consejo Nacional de Investigaciones Científicas y Técnicas, Conicet.

0020-1693/$ - see front matter © 2012 Elsevier B.V. All rights reserved.
http://dx.doi.org/10.1016/j.ica.2012.06.045

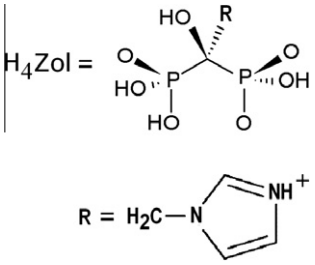

Scheme 1.

Paget's disease, tumor induced osteolysis; see, for instance, [12]). These compounds in general (and zoledronic acid, $H_4Zol = C_5H_{10}N_2O_7P_2$ in particular, see Scheme 1) are potentially good polydentate ligands prone to act as a bone "shield" by stacking into the skeleton, achieving therapeutic concentrations and thus inhibiting bone resorption by cellular effects on osteoclasts. In addition the well proved binding ability of zoledronic acid should enable the ligand to build unusual molecular architectures. We have already explored its binding behaviour to many metals of the first and second row, viz., K ([13], Na [14], Mg and Ca [15] where the anion appears in a number of different binding modes and protonation states.

Thus, as the result of our combined interest on magnetic properties of TM complexes, on one side, and on the multiply bridging properties of the zoledronate ligand on the other, we investigated the chemistry of Mn(II) and Fe(III) zoledronate compounds to end up with two complexes of fairly diverse nature, which we present herein. The first complex, formulated as $Mn(H_3Zol)_2(H_2O)_2$ (I), consists of a rather simple dimeric structure, isomorphic to an already reported TM series and which behaves as an almost theoretical paramagnet down to extremely low temperatures. The second one is a fairly unique molecular iron cluster of a fascinating structural complexity formulated as $Fe(III)_{15}(HZol)_{10}(H_2Zol)_2$ $(H_2O)_{24}$ $(2/3Cl{:}1/3H_2O)_6{\cdot}7Cl{\cdot}65(H_2O)$ (II), which behaves as a weak antiferromagnetic aggregate.

2. Results and discussion

2.1. Structural results

Table 1 presents a summary of crystallographic and refinement data for both compounds, while Table 2 shows the coordination distances and Table 3 the most relevant H-bonding interactions for (I) and only the non conventional C–H···O ones for (II).

Table 2
Coordination distances for (I), (II) (Å).

(a) (**I**)			
Mn1–O4	2.1281 (19)	Mn1–O1W	2.222 (2)
Mn1–O1	2.171 (2)		
(b) (**II**)			
Fe1–O3F	1.991 (5)	Fe5–O10W	2.070 (5)
Fe1–O4C	2.002 (4)	Fe5–O5W	2.075 (6)
Fe1–O3D	2.014 (4)	Fe5–Cl2	2.335 (3)
Fe2–O1F	1.921 (4)	Fe6–O2C	1.918 (5)
Fe2–O1D	1.928 (5)	Fe6–O2F	1.972 (4)
Fe2–O1W	2.078 (5)	Fe6–O4F	1.974 (5)
Fe2–O3W	2.094 (5)	Fe6–O4E	2.000 (5)
Fe2–O2W	2.098 (4)	Fe6–O2E	2.006 (5)
Fe3–O5F^{i}	1.913(5)	Fe6–O7W	2.131 (5)
Fe3–O2D	1.940 (5)	Fe7–O1C	1.964 (5)
Fe3–O2B^{i}	1.971 (5)	Fe7–O5E	1.967 (6)
Fe3–O4D	1.990 (4)	Fe7–O3E	1.970 (4)
Fe3–O4W	2.150 (5)	Fe7–O8W	2.042 (5)
Fe4–O5D	1.923 (4)	Fe7–O9W	2.070 (5)
Fe4–O5C	1.965 (4)	Fe7–Cl3	2.248 (4)
Fe4–O3C	1.970 (5)	Fe8–O3A	1.964 (5)
Fe4–O2A	1.974 (5)	Fe8–O6D	1.966 (5)
Fe4–O4A	2.033 (5)	Fe8–O5A	1.991 (5)
Fe4–O11W	2.161 (5)	Fe8–O6W	2.059 (5)
Fe5–O3B	1.954 (5)	Fe8–O12W	2.069 (5)
Fe5–O6F	1.969 (5)	Fe8–Cl1	2.361 (2)
Fe5–O5B	1.998 (5)		

Compound (I) consists of isolated dimeric units built up around an inversion centre (Fig. 1), and tightly interconnected by H-bonding (Table 3). The Mn1 cation resides at the symmetry centre, surrounded by two chelating zoledronate anions and two water molecules, of which only one is, of course, independent. This (1:2:2:0) cation:anion:$water_{coord.}$:$water_{solv.}$ pattern has already been found in some transition metal zoledronate complexes, the present structure being isomorphous to the Co and Ni [16] and Zn [17] isologues, for what only a very brief discussion of points usually left aside will be included here. The rather regular octahedron built up around the cation presents a Mn–O range of 2.128(2)–2.222(2) Å (Table 2a) and a (*cis*) O–Mn1–O angular range of 90 ± 5.47(9)°. Each zoledronate ligand displays its usual zwiterionic character, with a protonated imidazole ring, and two singly protonated phosphonates, with a resulting −1 total charge. This arrangement provides for due charge balance. P–OH distances

Table 1
Crystal and Refinement Data for (I), (II).

	(**I**)	(**II**)
Formula	$Mn(P_2O_7N_2C_5H_9)_2(H_2O)_2$	$Fe_{15}(P_2O_7N_2C_5H_7)_{10}(P_2O_7N_2C_5H_8)_2$ $(H_2O)_{24}[Cl_4{:}(H_2O)_2]{\cdot}7Cl{\cdot}65(H_2O)$
M_r	633.14	6097.96
a (Å)	7.4810 (15)	15.212 (2)
b (Å)	8.6030 (17)	19.277 (3)
c (Å)	9.7300 (19)	22.876 (3)
α (°)	105.32 (3)	65.252 (2)
β (°)	110.90 (3)	70.935 (2)
γ (°)	97.48 3	81.401 (2)
V (Å^3)	546.4 3	5757.0 (14)
μ = 0.99 mm^{-1}	0.99 mm^{-1}	1.33 mm^{-1}
Crystal size (mm)	0.22 × 0.18 × 0.14	0.14 × 0.12 × 0.11
Minimum, maximum Transmission	0.79, 0.87	0.82, 0.86
Reflections: measured, independent, $I > 2\sigma(I)$	5594, 2142, 1692	61599, 24828, 15077
R_{int}	0.023	0.087
$R[F^2 > 2\sigma(F^2)]$, $wR(F^2)$, S	0.034, 0.097, 1.06	0.074, 0.203, 1.04
Parameters	183	1528
$\Delta\rho_{max}/\Delta\rho_{min}$ (e Å^{-3})	0.51, −0.58	1.20, −0.72

Details in common: Triclinic, $P\bar{1}$, Z = 1, λ Mo Kα: 0.71073 (Å), Diffractometer: CCD Oxford Diffraction Gemini S Ultra; Absorption correction: multi-scan (CrysAlis PRO [29]); Temp: 291 K.

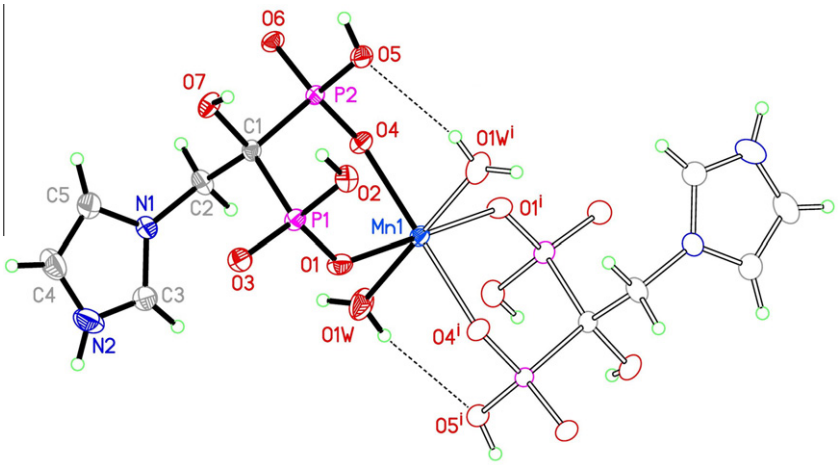

Fig. 1. Ellipsoid plot of (I), drawn at a 40% probability level, showing (in full lining and bonds) the asymmetric unit and (in empty ellipsoids and bonds) the symmetry related part completing the dimer. Symmetry codes: (i) $-x+2$, $-y+1$, $-z+2$.

(mean: 1.574 (3)Å) are, as expected, significantly longer than P–O (mean: 1.506 (8)Å), in agreement with what found in related structures (*viz.*, [18–20]. The phosphonate groups present an "eclipsed" conformations when viewed in the P1···P2 direction with a nearly planar O3–P1–C1–P2–O6 disposition (mean deviation from the plane 0.014 Å).

The dimers interact actively through H-bonding, with all available O–H's and N–H's taking part. These interactions are intercrossed, and accordingly define a tight 3D network In particular, the bond involving H1WA (Table 3a, 1st entry and Fig. 1) is intramolecular and provides to the dimer cohesion but all the remaining ones generate chains oriented along different directions, viz., the one involving H1WB (2nd entry) runs along [1 0 0], the H-bonds involving H_2O and H_7O (3rd–4th entries) generate 1D structures along [1 1 1]; the H_5O interaction (5th entry), a chain parallel to [1 1 0] while the H_2N one (6th entry), along [1 0 1].

Compound (II) consists of a centrosymmetric cluster with 15 Fe(III) cations (one of them at the inversion centre), 12 zoledronate anions, in different protonation states and 26 coordinated water molecules, 24 of which show full occupancy and the remaining 2 share 6 coordination sites with 4 chlorine anions. There are in addition 7 unbound chlorine counterions and 65 hydration water molecules as partially occupied hydration water molecules and their number adjusted as 65(H_2O), in order to match the chemical and TGA analysis (see Refinement section for details).

It is worth emphasizing that a search in both the Inorganic (ICSD [21]) and Organic (CSD [22]) data bases disclosed that the reported structures having Fe(III) as cationic centres bridged by PO_3 groups are polymeric in an overwhelming number of cases: no exceptions were found in the CSD and only three compounds of low nuclearity (2–4) out of a total of 48 structures were detected in the ICSD. So, Fe(III)–PO_3 clusters are extremely rare and the present one may be the first one reported.

Fig. 2a presents a (labelled) view of the asymmetric unit of the complex, representing the independent part of a centrosymmetric cluster; Fig. 2b complements this with a view of an (unlabelled) complete cluster. The general shape is that of a 6 arm propeller with a Fe(III) cation (Fe1) at its center and the FeO_6 coordination polyhedra (hereafter CP's) built up around Fe2, Fe2^{i} located above and below this central point and defining some sort of "paddle-wheel axis" perpendicular to the wheel plane. Around this axis there is a an almost perfect circular structure formed by the Fe3, Fe4, Fe6 CP's (plus their centrosymmetric counterparts Fe3^{i}, Fe4^{i}, Fe6^{i}, (i): $1-x$, $1-y$, $1-z$) to which the "paddles" defined by the Fe5, Fe7, Fe8, Fe5^{i}, Fe7^{i}, Fe8^{i} CP's attach. Fig. 3a shows a simplified view of this inorganic core, where the organic imidazole group has been excluded, for clarity. Even if all the Fe(III) CP's are FeO_6 octahedra, in each one of the different "zones" described these CP's have different characteristics taking into account the origin of the O's involved. Thus, the central CP around Fe1 is unique, with all its O ligands coming from six different BP groups (C, D, F, C^{i}, D^{i}, F^{i}). Second in hierarchy regarding BP involvement are those from the circular zone (Fe3, etc.) with five oxygens from three different BPs and one aqua; those from the external paddle zone (Fe5, etc.) follow, with two BP O's, two fully occupied aqua and a third, partially occupied oxygen sharing the site with a Chlorine anion. Finally, the axial CP's around Fe2, Fe2^{i}, are built up by three BP O's and three fully occupied aqua. Table 2b gives a detailed survey of Fe–O bond distances.

The six independent BP units bind as two differentiated groups: Units C, D and F have all six oxygens mono coordinated; units A, B and E have four, and two uncoordinated ones (O1 and O6) which can be good candidates for protonation. The ligands present conformations leaned towards the "eclipsed" side, as viewed in the P1···P2 direction, with O1–P1–C1–P2 and P1–C1–P2–O6 torsion angles differing in the range 12.1 (1)–23.2 (1)°, for units B and F, respectively. An ideally eclipsed conformations would require 0°, while a perfectly staggered one, 60°.

The whole inorganic nucleous shown in Fig. 3a can be envisaged as composed by elemental motives involving Fe(III) cations and O–P–O groups (hereafter OPO's) from BP anions. These units are in fact just simple (or multiple) closed loops characterized by a common formula of the type $(Fe\cdots OPO)_n$, $n = 2,3,4$, interlinked in such a way that any cation in the nucleous is connected with any of its nearest neighbors via one of these OPO bridges and O atoms binding to just one cation.

The smallest loop ($n = 2$), composed of two Fe atoms and bridged by two different OPO groups appear in the structure only as aggregates of conjugated triplets sharing their Fe ends, to end up in a triply bridged dinuclear species. There are two different types of this elemental unit in the structure, presenting the same connectivity but different geometries. Unit A1, (Fig. 3a) appears in the external "paddle" region, and the six groups of this sort display extremely similar Fe···Fe distances: Fe3···Fe5^{i}: 4.616 (1); Fe4···Fe8: 4.614 (1); Fe6···Fe7: 4.574 (1). The second one of these triply bridged entities (Unit A2) as well as the remaining motives with $m = 3$, 4 appear quite deep in the cluster core, in a substructure resembling a BCC motive of Fe(III) cations and OPO connectors, In Fig. 4a–d we sketch this pseudo BCC motive, highlighting in turn the different $(Fe\cdots OPO)_n$, $n = 2,3,4$ embedded loops which

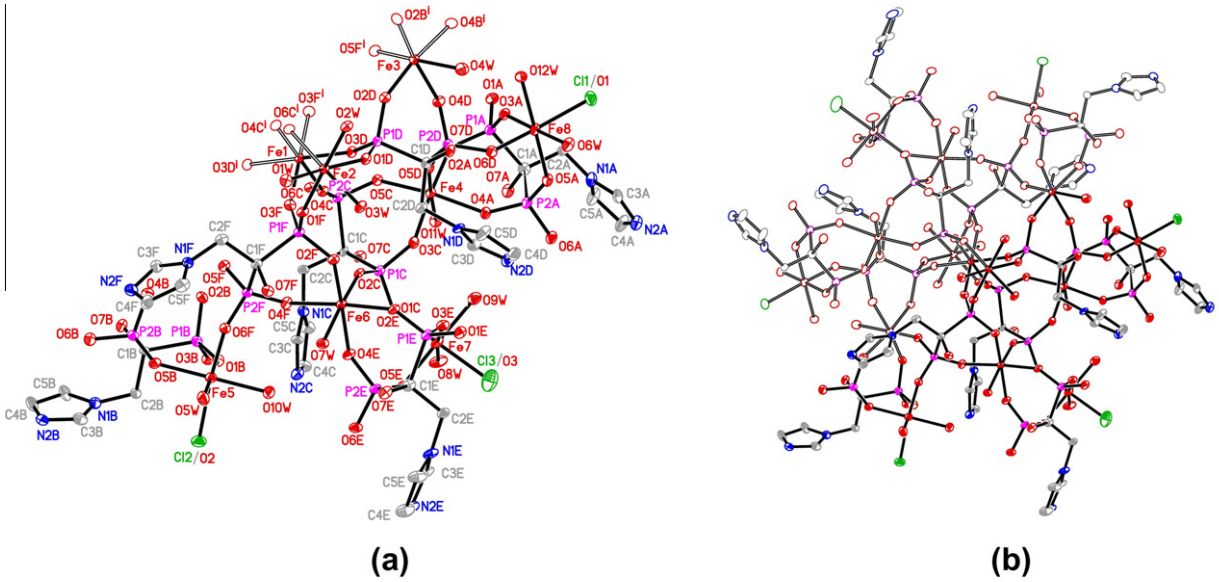

Fig. 2. (a) Ellipsoid plot of (II), drawn at a 40% probability level, showing the asymmetric unit and labels used. (b) A complementing view of the complete cluster. Symmetry codes: (i) $-x+1, -y+1, -z+1$.

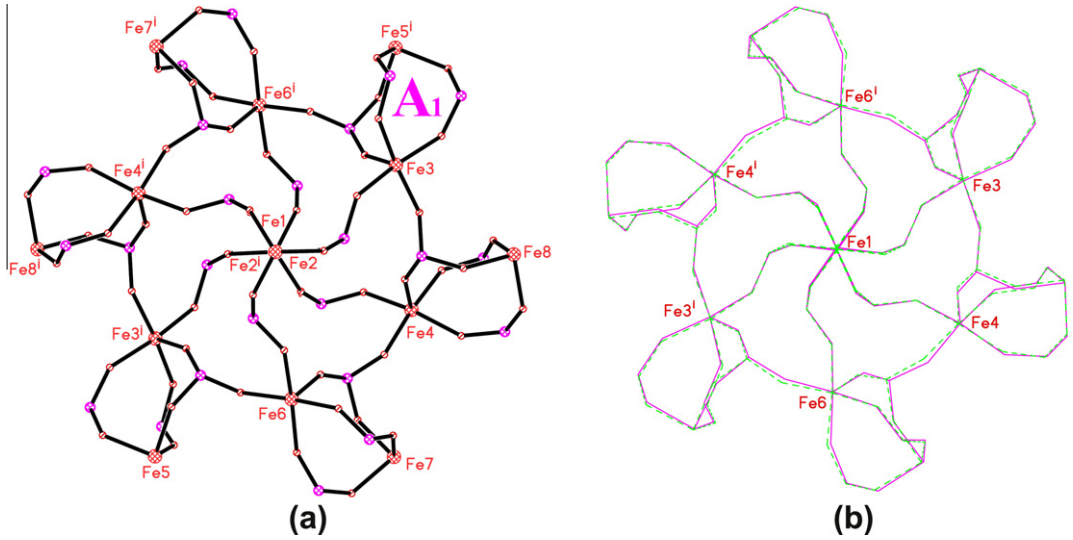

Fig. 3. (a) A view of the inorganic nucleous, with the organic part removed, for clarity. Labelled as A1: one of the $(Fe\cdots OPO)_2$ motives building up the structure (see text). (b) Fitting of the inorganic nucleous with its -3 image.

this entanglement gives rise to. Even if loops with $n > 4$ do in fact exist, they are the result of those already described, and will not be considered here.

Fig. 4a shows (highlighted) the second type of the triply bridged entities (Unit A2). There are two centrosymmetrically related moieties of this sort, sharing atom Fe1 and stretching along the [1 1 1] diagonal of the BCC cube; as stated, they define the paddlewheel axis, with a $Fe2^{i}\cdots Fe1\cdots Fe2$ distance of $2 \times 4.688\ (1)$ Å.

Fig. 4b presents in turn the $n = 3$ loop B, of which there are 6 equivalent moieties, while 4c, 4d show two different types of loops for $n = 4$ (C1 and C2), with 4 equivalent representatives for the former and 6 for the latter.

These $(Fe\cdots OPO)_n$ loops are rather unusual; the only ones found in related structures are the simple loops with $n = 2$ [23,24] and $n = 3$ [25]. As a result, the triple $n = 2$ bridge, and the larger $n = 4$ loop are so far unreported.

All these metric singularities are manifestations of a unique and striking non-crystallographic symmetry adorning the cluster and strongly suggested in Fig. 3a; in fact, the whole assembly presents an almost perfect -3 symmetry, with Fe1 at the center. This can be easily assessed by overlapping the molecular nucleous shown in Fig. 3a with itself after a 120° rotation followed by an inversion with respect to Fe1; the surprising result is graphically presented in Fig. 3b, and quantified by the low average misfit value, 0.128 (7) Å.

The charge distribution on the iron sites as suggested by the bond distances shown in Table 2b appear as quite even, with cations Bond Valences [26] ranging from 2.90, for Fe5, to 3.10, for Fe7. This gives a total cationic charge of 45+ per cluster. The anionic charge effectively found and which (partially) compensates it comes from the Cl^- groups (4 of them bound, but disordered, with a total charge of 4−, and 7 of them free and fully occupied, providing 7−). Thus the 45–11 = 34 electrons left could come from the $H_nZol^{(4-n)-}$ anions, a situation attainable, for instance, through the proposed formulation $(HZol)_{10}^{3-}$ $(H2Zol)_2^{2-}$.

Due to the X-ray data quality limitations, O–H···O interactions could not be identified. Only the weak, non-conventional C–H···O

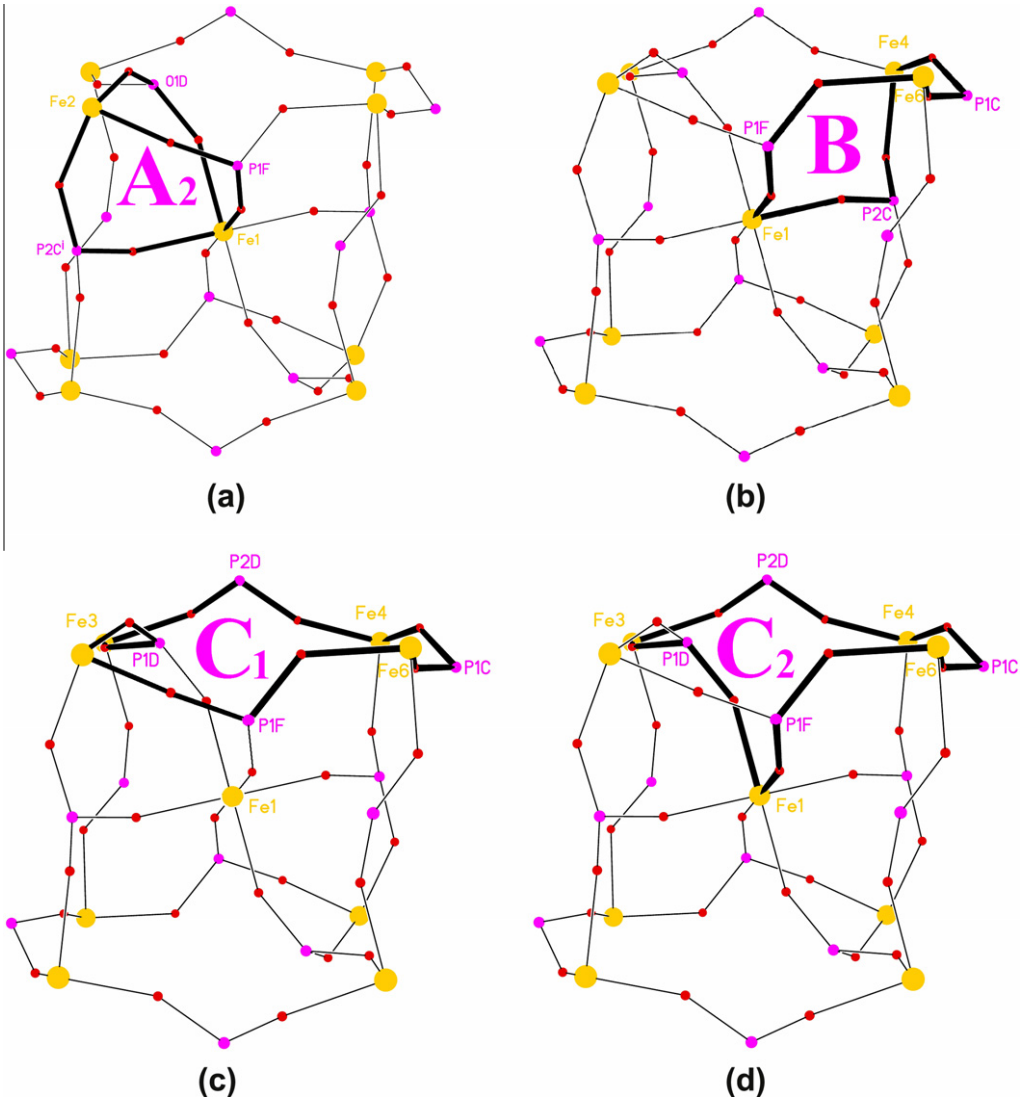

Fig. 4. Some of the remaining $(Fe\cdots OPO)_n$ entangled motives building up the structure (a) A2, $n = 2$; (b) B, $n = 3$; (c) C1, $n = 4$; (d) C2, $n = 4$.

Table 3
Hydrogen-bond interactions for (I) (Å, °).

D–H···*A*	*D*–H	H···*A*	*D*···*A*	*D*–H···*A*
(a) (I)				
O1W–H1WA···O5^{i}	0.85 (1)	2.35 (3)	3.056 (3)	141 (5)
O1W–H1WB···O6^{ii}	0.84 (1)	1.89 (1)	2.724 (3)	173 (5)
O2–H2O···O3^{iii}	0.85 (1)	1.82 (1)	2.655 (3)	170 (4)
O7–H7O···O3^{iii}	0.85 (1)	2.10 (2)	2.909 (3)	159 (3)
O5–H5O···O6^{iv}	0.84 (1)	1.74 (1)	2.580 (3)	172 (4)
N2–H2N···O1^{v}	0.85 (1)	1.88 (1)	2.723 (3)	169 (4)
Symmetry codes: (i) $-x+1, -y+1, -z+1$; (ii) $-x, -y+1, -z+1$; (iii) $-x, -y, -z$; (iv) $-x, -y, -z+1$; (v) $-x, -y+1, -z$.				
(b) (II)				
C3C–H3CA···O4F	0.93	2.25	3.121 (10)	156
C3D–H3DA···O3C	0.93	2.37	3.254 (10)	159
C3F–H3FA···O4D^{i}	0.93	2.29	3.188 (11)	163
Symmetry code: (i) $-x+1, -y+1, -z+1$.				

ones could be found, the most significant of which are presented in Table 3b. There are, however, some general features worth mentioning, viz.: the cluster display their flat side parallel to (1 1 1) with the Fe2–Fe2^{i} axis just 1.5° out of the plane normal. The clusters aggregate in this (1 1 1) planes with a striking "hexagonal" distribution, as shown in Fig. 5a, where only the clusters are drawn (counterions and solvates omitted). The pseudosymmetry is apparent, and reinforced by some numerical data, viz.: range of cluster centroid distances (the hexagon "sides"): 22.700 (3)–22.964 (3) Å; range of hexagon "internal angles": 60.0 ± 0.7°.

This pseudohexagonal symmetry, however, does not propagate along the [1 1 1]* reciprocal direction normal to the plane, as the hexagonal neighboring planes, one d_{111} spacing apart (12.717 Å) appear shifted in projection. Fig. 5b shows three consecutive

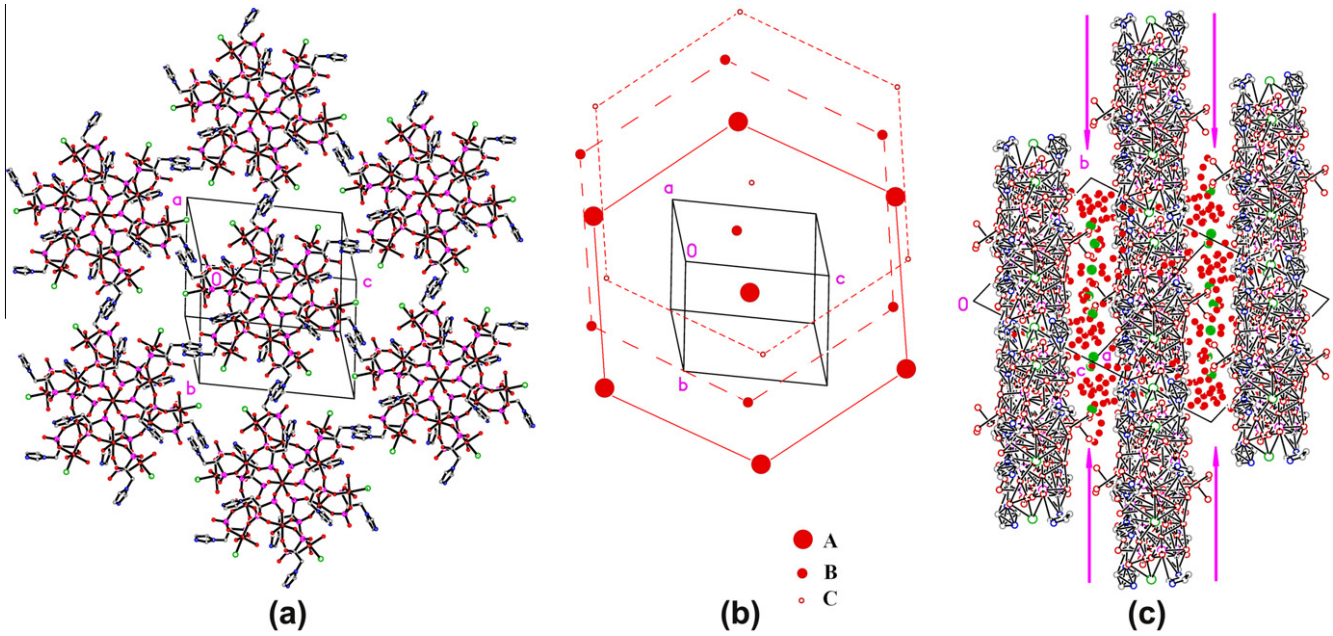

Fig. 5. Packing diagrams of (II) (a) a (1 1 1) layer, showing the pseudohexagonal disposition of the clusters. NOTE: in spite of the deceiving resemblance in the Figure, there are no $\pi\cdots\pi$ interactions linking adjacent imidazole rings. (b) A sketch showing the shift of these (1 1 1) reference planes (A) when moving one d_{111} spacing (up (B) and down (C)) along the [−1 0 1] direction, normal to the planes. (c) A [−1 0 1] projection showing the counterions and solvates stuffing the free space between planes.

planes, the macromolecules represented by their central Fe1 atom and where this "vertical" misfit is apparent. Finally, a packing view along [−1 0 1] (Fig. 5c), at right angles to the latter projection, shows the way in which counterions and solvates locate (See arrows) "stuffing" the empty space between the (dense) cluster planes parallel to (1 1 1), seen in projection. The interatomic proximity is apparent, suggesting a strong plane-to-stuff interaction stabilizing the structure.

It is well known that 15 is one of the "magic numbers" for metal conglomerates, and Fe_{15} is one of the most studied Fe metallic clusters [27]. A nearest neighbors analysis predicts for the topology of such a Fe_{15} cluster a "bcc-like" distribution [28], with one Fe at the center of a reference cell, eight nearest neighbors at the vertices and the remaining six at the centres of the neighboring cubes.

Even if this applies to isolated metal atoms, an analysis of the spatial distribution of the 15 Fe(II) ions in (II) surprisingly shows an unexpected similarity in the ion distribution.

The cluster in (II) can be described with Fe1 located at the center, on a crystallographic inversion centre, eight nearest neighbors (which we shall call "the first shell"), with a Fe···Fe1 distance range of 4.67 A to 6.37 A) and six next nearest neighbors ("second shell": with a tight Fe···Fe1 distance range: 8.18 A to 8.23 A) following some sort of distorted bcc arrangement, as described below: when comparing the experimental distribution with the theoretical one, there are obvious differences due to metric and angular distortions, but there is a second, more interesting difference which, paradoxically enhances the similarity: the atoms in the "second shell" in (II) are not located on the body center of the nearest neighboring cells (those sharing a face with the reference cube) but on the body center of 6 (out of a total of 12) of the second nearest neighboring ones (those sharing one edge with the reference cube). This topology, consistent with the presence of spin frustration arising from competing exchange interactions, is obviously less symmetric, but compatible the predicted bcc one, a perhaps could be considered as an alternative model for Fe_{15} clusters.

2.2. Magnetic properties

Magnetic susceptibility data for polycrystalline samples of both compounds were collected in the temperature range 2–250 K under an applied magnetic field of 1T.

The corresponding plots of X_MT are given in Fig. 6a and b, while the associated X_M^{-1} versus T plots (with the corresponding Curie–Weiss fitting down to15 K in (I) and 100 K in (II)) are shown as insets (X_M: molar magnetic susceptibility).

Both pictures (main figure and inset) show the materials to be paramagnetic in the quoted ranges. In the case of (I) the value of X_MT at 250 K (~3.95 $cm^3\ mol^{-1}$ K) is in reasonable agreement with the expected one for uncoupled Mn(II) ions (4.375 $cm^3\ mol^{-1}$ K), while values of X_M^{-1} follow a Curie–Weiss behaviour [$X_M = C/(T-\theta)$] above ~15 K, with $C = 3.97\ cm^3\ mol^{-1}$ K and $\theta = 1.3$ K (Fig. 6a, inset). The Curie constants are also consistent with one uncoupled Mn(II) ion with $g = 2$, while the positive Weiss constant suggests a tendency to small ferromagnetic interactions.

Compound (II), in turn, presents a X_MT per Fe(III) value with a tenfold drop in the 250 K–2 K range (from 3.3 $cm^3\ mol^{-1}$ K down to 0.35 $cm^3\ mol^{-1}$ K), with a sensibly increased downwards rate below $T \sim 50$ K. The room temperature value (~3.30 $cm^3\ mol^{-1}$ K) is sensibly smaller than the expected one for completely uncoupled Fe(III) with $g = 2$ (4.375 $cm^3\ mol^{-1}$ K), which in addition to the marked decrease upon cooling suggests the presence of antiferromagnetic interactions within the cluster. X_M^{-1} values [$X_M = C/(T + T_n)$] follow a Curie–Weiss behaviour above $T \sim 100$ K with $C = 3.55\ cm^3\ mol^{-1}$ K and $T_n = -19.6$ K (Fig. 6b, inset), in agreement with the presence of dominant antiferromagnetic interactions in the cluster.

Complementing the magnetic susceptibility measurements, the dependence of the sample magnetization with the applied magnetic field was determined for both compound at selected temperatures (see Fig. 7a and b). It should be noted that for complex (I) the experimental data lay slightly above the expected ones for uncoupled Mn(II) ions (Fig. 7a, $T = 2$ K), another hint for the presence of small ferromagnetic interactions.

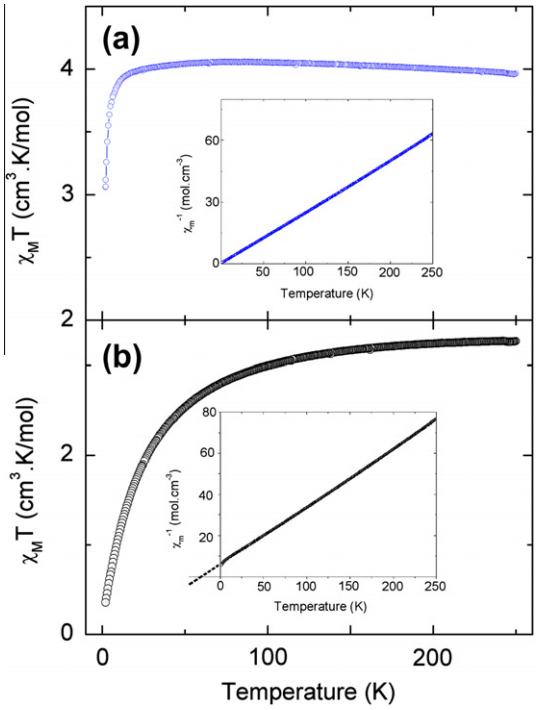

Fig. 6. Temperature dependence of the $X_M T$ product for compound I (a) and II (b). In the insets, the linear behaviour of the inverse of X_M, following a Curie–Weiss law in both cases.

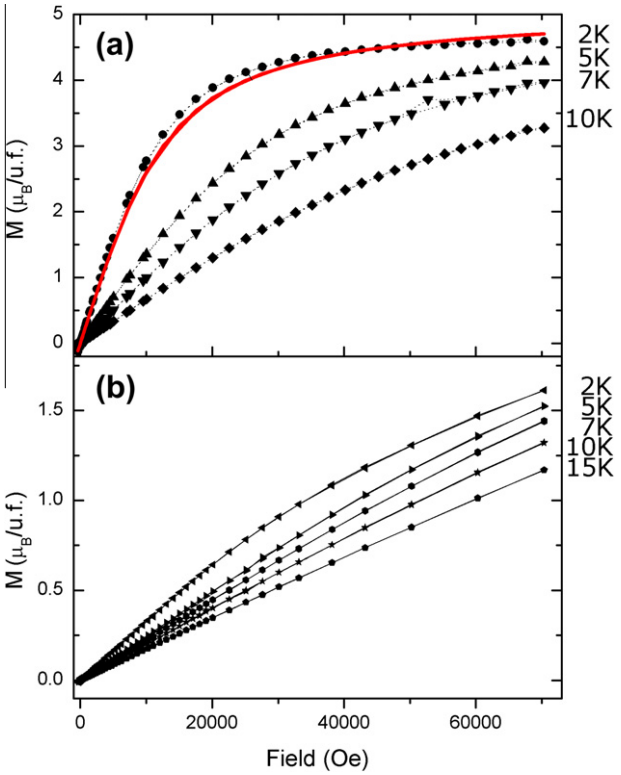

Fig. 7. Field dependence of magnetization at different temperatures. (a) Compound (I). At T = 2 K a comparison is made between the experimental results (black dots) and the curve calculated with a Langevin function (full red line). (b) Compound (II). The linear dependence observed can be indicative of the frustration of the system. (For interpretation of the references to color in this figure legend, the reader is referred to the web version of this article.)

Experimental data for (II) evidence a low value of the magnetization even for temperatures as low as 2 K and extremely high fields (7T), in agreement with antiferromagnetic interactions between Fe(III) ions.

Summarizing, we have presented two new zoledronate complexes of fairly diverse nature, the simple dimeric $Mn(Zol)_2.(H_2O)_2$(I), isomorphic to an already reported TM series and which behaves as an almost theoretical paramagnet down to extremely low temperatures, where some ferromagnetic interactions are glimpsed, and a rather unique molecular iron cluster of a fascinating structural complexity formulated as $Fe(III)_{15}(HZol)_{10}(H_2Zol)_2(H_2O)24\,(2/3Cl{:}1/3H_2O)_6{\cdot}7Cl{\cdot}65(H_2O)$ (II), which behaves as a weak antiferromagnetic aggregate.

3. Experimental

3.1. Materials and methods

All chemicals were reagent-grade purity purchased from Aldrich and used as received. Elemental Analyses (C, N, H) were performed on a Carlo_/Erba EA 1108 instrument. Thermogravimetric analyses were recorded on a Shimadzu DTG50 thermal analyzer under an atmosphere of air at a heating rate of 10 °C min^{-1}.

Single crystal X-ray data were collected at room temperature (291(2) K) on an Oxford Diffraction Gemini CCD diffractometer, with graphite monochromated Mo Kα radiation (λ = 0.71073 Å).

Magnetic measurements were carried out on polycrystalline samples with a Quantum Design SQUID MPMS magnetometer apparatus working in the range 2–250 K under magnetic fields of 1T. The magnetization curves were recorded at 2 K at fields ranging from 0 to 7T.

3.2. Synthesis

The manganese(II) and ferric(III) complexes of zoledronic acid were synthesized by reacting 3 ml water solutions of each metal salts, $Mn(NO_3)_2$ (0.10 mmol, 0.0251 g) and $FeCl_3$ (0.10 mmol, 0.0162 g) with 3 ml hot (80C) water solution of zoledronic acid (0.10 mmol, 0.0272 g) in 1:1 M ratio, in a small beaker. Both solutions were acidified with concentrated HCl, adjusting to a final pH = 1.

Large, pale rose crystals for the Mn(II) complex and small redish crystals of the Fe(III) compound were obtained after very slow evaporation at room temperature (weeks and months, respectively).

3.3. X-ray crystallography

The structures were primarily solved by direct methods and completed by difference Fourier synthesis. The software used was: data collection, cell refinement and data reduction CrysAlis PRO [29]; structure resolution, refinement, graphics: SHELXS97, SHELXL97, SHELXTL [30].

In structure (I) H atoms attached to O and N were found in a difference Fourier map, and further refined with restrained distances (O–H: 0.85, H···H: 1.35, N–H: 0.85 Å) and free U_{iso}. In structure (II), they were not found and were accordingly not included in the model. In both structures, H's attached to C were placed at calculated positions (C–H: 0.93 Å; C–H_2: 0.97 Å) and allowed to ride. Displacement factors were taken as $U(H)_{isot}$ = 1.2/1.5 U_{host}.

Structure (II) posed a problem both in resolution and in refinement: in addition to the well defined cationic molecular group and complementing isolated counterions the difference map showed a very large number ill defined of peaks. An attempt of using the SQUEEZE procedure in PLATON [31] did not proved satisfactory in reducing the general background peaks jeopardizing the molecular refinement. Thus, the solution adopted was to model these

peaks as unrelated, depleted water solvates with fixed occupation factors in the range 0.80–0.20 leading to reasonable displacement factors and restrained in number to match what obtained from chemical and TGA analysis [32]. This artifact enabled the refinement of the core and to unveil the details of the very singular structure we describe. There are three terminal sites in the cluster, bound to Fe, which have occupational disorder, being shared by O and Cl species. The disorder was evidenced by the abnormal anisotropic displacement factors obtained when the sites were considered fully occupied by Cl, as suggested by the coordination distances obtained (Final O/Cl occupancies: 0.13/0.87 (2), 0.29/0.71 (2), 0.58/0.42 (2), which were kept fixed at the final stages of refinement).

Acknowledgements

Zoledronic acid was provided by GADOR ARGENTINA, S.A. and is gratefully acknowledged. We also acknowledge PIP-11220090100889 and ANPCyT (Project No. PME 2006-01113) for the purchase of the Oxford Gemini CCD diffractometer and the Spanish Research Council (CSIC) for provision of a free-of-charge licence to the Cambridge Structural Database.

Appendix A. Supplementary material

CCDC 877546 and 877547 contains the supplementary crystallographic data for this paper. These data can be obtained free of charge from The Cambridge Crystallographic Data Centre via www.ccdc.cam.ac.uk/data_request/cif. Supplementary data associated with this article can be found, in the online version, at http://dx.doi.org/10.1016/j.ica.2012.06.045.

References

[1] R.H. Holm, P. Kennepohl, E.I. Solomon, Chem. Rev. 96 (1996) 2239.
[2] M. Yoshizawa, M. Tamura, M. Fujita, Science 312 (2006) 251.
[3] H. Hou, Y. Wei, Y. Song, L. Mi, M. Tang, L. Li, Y. Fan, Angew. Chem., Int. Ed. 44 (2005) 6067.
[4] R.W. Saalfrank, A.R. Scheure, I. Bernt, F.W. Heinemann, A.V. Postnikov, V. Schüunemann, A.X. Trautwein, M.S. Alam, H. Rupp, P. Müller, Dalton Trans. (2006) 2865.
[5] R. Sessoli, H.L. Tsai, A.R. Schake, S. Wang, J.B. Vincent, K. Folting, D. Gatteschi, G. Christou, D.N. Hendrickson, J. Am. Chem. Soc. 115 (1993) 1804.
[6] C. Cañada Vilalta, T.A. O'Brien, M. Pink, E.R. Davidson, G. Christou, Inorg. Chem. 42 (2003) 7819.
[7] M.D. Godbole, O. Roubeau, A.M. Mills, H. Kooijman, A.L. Spek, E. Bouwman, Inorg. Chem. 45 (2006) 6713.
[8] G.C. Dismukes, in: J. Reedijk (Ed.), Bioinorganic Catalysis, Marcel Dekker, New York, 1993, pp. 317 (Chapter 10).
[9] S. Mukhopadhyay, S.K. Mandal, S. Bhaduri, W.H. Armstrong, Chem. Rev. 104 (2004) 3981.
[10] G. Christou, D. Gatteschi, D.N. Hendrickson, R. Sessoli, MRS Bull. 25 (2000) 66.
[11] D. Gatteschi, R. Sessoli, J. Magn. Magn. Mater. 272 (2004) 1030.
[12] J.R. Green, J. Organomet. Chem. 690 (2005) 2439.
[13] E. Freire, D.R. Vega, R. Baggio, Acta Cryst. C66 (2010) m13.
[14] E. Freire, D.R. Vega, R. Baggio, Acta Cryst. C66 (2010) m122.
[15] E. Freire, D.R. Vega, R. Baggio, Acta Cryst. C66 (2010) m166.
[16] D.-K. Cao, Y.-Z. Li, L.-M. Zheng, Inorg. Chem. 46 (2007) 7571.
[17] E. Freire, D.R. Vega, Acta Cryst. E65 (2009) m1428.
[18] V.M. Coiro, D. Lamba, Acta Cryst. C45 (1989) 446.
[19] D. Vega, R. Baggio, M.T. Garland, Acta Cryst. C52 (1996) 2198.
[20] D. Vega, R. Baggio, O. Piro, Acta Cryst. C54 (1998) 324.
[21] ICSD (2011). Inorganic Crystal Structure Database. FIZ-Karlsruhe, Germany, and the National Institute of Standards and Technology (NIST), USA <http://www.fiz-karlsruhe.de/icsd.html>.
[22] F.H. Allen, Acta Cryst. B58 (2002) 380.
[23] E. Kostiner, J.R. Rea, Inorg. Chem. 13 (1974) 2876.
[24] P.B. Moore, T. Araki, Am. Mineral. 59 (1974) 964.
[25] H.N. Ng, C. Calvo, Can. J. Chem. 53 (1975) 2064.
[26] I.D. Brown, The Chemical Bond in Inorganic Chemistry: The Bond Valence Model, Oxford University Press, 2002.
[27] M. Sakurai, K. Watanabe, K. Sumiyama, K. Suzuki, J. Phys. Soc. Jpn. 67 (1998) 2571.
[28] E.K. Parks, G.C. Nieman, L.G. Pobo, S.J. Riley, J. Chem. Phys. 88 (1988) 1622.
[29] Oxford Diffraction, CrysAlis PRO, version 171.33.48, Oxford Diffraction Ltd., Abingdon, Oxfordshire, England, 2009.
[30] G.M. Sheldrick, SHELXL-97, SHELXS-97, SHELXTL, Acta Cryst. A64 (2008) 112.
[31] A.L. Spek, J. Appl. Cryst. 36 (2003) 7.
[32] Anal. for (I) $C_{10}H_{22}MnN_4O_{16}P_4$: Calc.: C 18.97; H 3.50; N 8.85%; Found: C 19.00; H 3.61; N 8.82%. Anal. for (II) $C_{60}H_{268}Cl_{11}Fe_{15}N_{24}O_{175}P_{24}$: Calc. C 11.89; H 3.79; N 5.55% Found: C 11.7; H 3.9; N 5.4%. TGA of structure (II) was carried out from room temperature up to 600 °C. A broad peak amounting for a weight loss of 24% of the total mass (range: 310 °C–390 °C) was interpreted as the combined loss of the 7 chlorine counterions (4%) and an undetermined number of solvate water molecules (20%). This latter percentage allowed to fix the water solvate content to about 65 units per formula. This final number was used in the restrained X-ray refinement.